Online Supplement for the Paper

An Automated Intensity-Modulated Radiation Therapy Planning System

Shabbir Ahmed, Ozan Gozbasi, Martin Savelsbergh

H. Milton Stewart School of Industrial and Systems Engineering, Georgia Institute of Technology, Atlanta, Georgia 30332, USA, {sahmed@gatech.edu, ozan@gatech.edu, mwps@isye.gatech.edu}

Ian Crocker, Tim Fox, Eduard Schreibmann

Department of Radiation Oncology, Emory University School of Medicine, 1365 Clifton Road NE Atlanta, Georgia 30322, USA, {ian@radonc.emory.org, tim@radonc.emory.org, edi@radonc.emory.org}

1. Proof of Proposition 1

Proposition 1 *Given $\alpha_s \in (0,1)$, if there exists a c_s such that*

$$c_s - \frac{1}{(1-\alpha_s).V_s} \sum_{j=1}^{V_s} (c_s - z_{js})^+ \geq PD_s \tag{1}$$

then

$$\text{coverage}(s) \geq \alpha_s. \tag{2}$$

Proof

For simplicity of exposition, we assume that α_s is such that $\alpha_s V_s$ is a positive integer. Let D^{α_s} be such that

$$\sum_{j=1}^{V_s} \mathbb{I}_+(z_{js} - D^{\alpha_s}) = \alpha_s V_s.$$

Then the coverage requirement (2) is equivalent to

$$D^{\alpha_s} \geq PD_s.$$

We prove the result by showing that if there exists c_s satisfying (1) then we must have $D^{\alpha_s} \geq PD_s$.

Note that

$$D^{\alpha_s} \geq D^{\alpha_s} - \frac{1}{(1-\alpha_s).V_s} \sum_{j=1}^{V_s} (D^{\alpha_s} - z_{js})^+,$$

which follows simply from the fact that $(D^{\alpha_s} - z_{js})^+$ is non-negative. We claim that

$$D^{\alpha_s} - \frac{1}{(1-\alpha_s).V_s} \sum_{j=1}^{V_s} (D^{\alpha_s} - z_{js})^+ \geq c_s - \frac{1}{(1-\alpha_s).V_s} \sum_{j=1}^{V_s} (c_s - z_{js})^+ \quad \forall\ c_s \in \Re.$$

Suppose this is not true. Then, there exists c_s^* such that

$$D^{\alpha_s} - \frac{1}{(1-\alpha_s).V_s}\sum_{j=1}^{V_s}(D^{\alpha_s} - z_{js})^+ < c_s^* - \frac{1}{(1-\alpha_s).V_s}\sum_{j=1}^{V_s}(c_s^* - z_{js})^+. \tag{3}$$

Consider the following two cases.

Case 1: suppose that $c_s^* \leq D^{\alpha_s}$. Then the right-hand-side (rhs) of (3) is

$$\begin{aligned}
\text{rhs} &= c_s^* - \frac{1}{(1-\alpha_s).V_s}\sum_{j:\ c_s^* > z_{js}}(c_s^* - z_{js}) \\
&= c_s^* - \frac{1}{(1-\alpha_s).V_s}\left[\sum_{j:\ D^{\alpha_s} > z_{js}}(c_s^* - z_{js}) - \sum_{j:\ c_s^* \leq z_{js} < D^{\alpha_s}}(c_s^* - z_{js})\right] \\
&= c_s^* - \frac{1}{(1-\alpha_s).V_s}\sum_{j:\ D^{\alpha_s} > z_{js}}(c_s^* - z_{js}) + \underbrace{\frac{1}{(1-\alpha_s).V_s}\sum_{j:\ c_s^* \leq z_{js} < D^{\alpha_s}}(c_s^* - z_{js})}_{\leq 0} \\
&\leq c_s^* - \frac{1}{(1-\alpha_s).V_s}\sum_{j:\ D^{\alpha_s} > z_{js}}(c_s^* - D^{\alpha_s} + D^{\alpha_s} - z_{js}) \\
&= c_s^* - \frac{1}{(1-\alpha_s).V_s}\sum_{j=1}^{V_s}(D^{\alpha_s} - z_{js})^+ - \frac{1}{(1-\alpha_s).V_s}\sum_{j:\ D^{\alpha_s} > z_{js}}(c_s^* - D^{\alpha_s}) \\
&= c_s^* - \frac{1}{(1-\alpha_s).V_s}\sum_{j=1}^{V_s}(D^{\alpha_s} - z_{js})^+ - (c_s^* - D^{\alpha_s}) \\
&= D^{\alpha_s} - \frac{1}{(1-\alpha_s).V_s}\sum_{j=1}^{V_s}(D^{\alpha_s} - z_{js})^+ = \text{lhs},
\end{aligned}$$

where lhs is the left-hand-side of inequality (3), hence a contradiction. Note that the last step in the above follows from the definition of D^{α_s} which implies $|\{j:\ z_{js} < D^{\alpha_s}\}| = (1-\alpha_s)V_s$.

Case 2: suppose that $c_s^* > D^{\alpha_s}$. Then the right-hand-side (rhs) of (3) is

$$\begin{aligned}
\text{rhs} &= c_s^* - \frac{1}{(1-\alpha_s).V_s} \sum_{j:\ c_s^* > z_{js}} (c_s^* - z_{js}) \\
&= c_s^* - \frac{1}{(1-\alpha_s).V_s} \left[\sum_{j:\ D^{\alpha_s} > z_{js}} (c_s^* - z_{js}) + \sum_{j:\ D^{\alpha_s} \le z_{js} < c_s^*} (c_s^* - z_{js}) \right] \\
&= c_s^* - \frac{1}{(1-\alpha_s).V_s} \sum_{j:\ D^{\alpha_s} > z_{js}} (c_s^* - z_{js}) - \underbrace{\frac{1}{(1-\alpha_s).V_s} \sum_{j:\ D^{\alpha_s} \le z_{js} < c_s^*} (c_s^* - z_{js})}_{\ge 0} \\
&\le c_s^* - \frac{1}{(1-\alpha_s).V_s} \sum_{j:\ D^{\alpha_s} > z_{js}} (c_s^* - D^{\alpha_s} + D^{\alpha_s} - z_{js}) \\
&= D^{\alpha_s} - \frac{1}{(1-\alpha_s).V_s} \sum_{j=1}^{V_s} (D^{\alpha_s} - z_{js})^+ = \text{lhs},
\end{aligned}$$

where the last step is identical to Case 1. Hence we again have a contradiction.

Thus if there exists c_s satisfying (1) then

$$D^{\alpha_s} \ge D^{\alpha_s} - \frac{1}{(1-\alpha_s).V_s} \sum_{j=1}^{V_s} (D^{\alpha_s} - z_{js})^+ \ge c_s - \frac{1}{(1-\alpha_s).V_s} \sum_{j=1}^{V_s} (c_s - z_{js})^+ \ge PD_s$$

completing the proof.

2. Dose Distribution Images

We show three sets of dose distribution images in Figures 1, 2, and 3 for the brain case, the head and neck case, and the prostate case, respectively. For each case, we present three slices corresponding to the three treatment plans: (1) a plan with equi-spaced beams obtained by solving the model, but without parameter search, (2) a plan with equi-spaced beams obtained by solving the model incorporating parameter search, and (3) a plan with optimized beam angles obtained by solving the model incorporating parameter search. The prescription dose is shown as red colorwash with 75, 50 and 25% of prescription dose shown as yellow, green and blue colorwash. CT axial images 1, 2, and 3 represent inferior, mid and superior slices through the target volume. In all three cases, plan c (obtained by integrating parameter search with careful selection of beam angles) is preferable. In particular, in the brain case (Figure 1) the hot beamlet effect on the left side of the patient evident in plans a and b is minimized in plan c. In the head and neck case (Figure 2), for plan a, we observe significant 75% dose leaking (yellow colorwash) out of the tumor area in all three slices. On plan

b, this is improved but we have a hot beamlet effect right next to the brainstem on slice 3 and this is not preferable. Plan c seems to be much better with tighter conformity of the dose including slice 3 where the PTV comes closer to brainstem. Similarly for the prostate case (Figure 3), plans a and b have hot spots along the beam directions which is not preferable. Plan c tends to pull in the high dose closer to the prostate.

3. Comparison to a Scoring-Based Approach

We computed beam angle configurations for the cases using pBEV scores and our proposed scores, and then performed fluence map optimization. Multiple solutions are produced for each case by varying the number of beam angles. The results for brain case, head and neck case, and prostate case are presented in Tables 1, 2 and 3; respectively.

	6 beams		7 beams		8 beams		9 beams	
	pBEV	Proposed Scheme	pBEV	Proposed Scheme	pBEV	Proposed Scheme	pBEV	Proposed Scheme
Coverage	0.954	0.963	0.962	1.000	0.979	1.000	1.000	1.000
Conformity	1.245	1.214	1.279	1.144	1.233	1.125	1.082	1.099
Coldspot	0.919	0.956	0.928	1.000	0.947	1.000	1.000	1.000
Hotspot	1.078	1.078	1.078	1.078	1.078	1.078	1.078	1.078

Table 1: Brain case comparison to pBEV

	6 beams		7 beams		8 beams		9 beams	
	pBEV	Proposed Scheme	pBEV	Proposed Scheme	pBEV	Proposed Scheme	pBEV	Proposed Scheme
Coverage	0.962	0.968	0.968	0.971	0.968	0.974	0.968	0.973
Conformity	1.253	1.219	1.247	1.243	1.199	1.232	1.177	1.162
Coldspot	0.337	0.301	0.327	0.320	0.351	0.310	0.360	0.314
Hotspot	1.200	1.200	1.200	1.200	1.200	1.200	1.200	1.200

Table 2: Head and Neck case comparison to pBEV

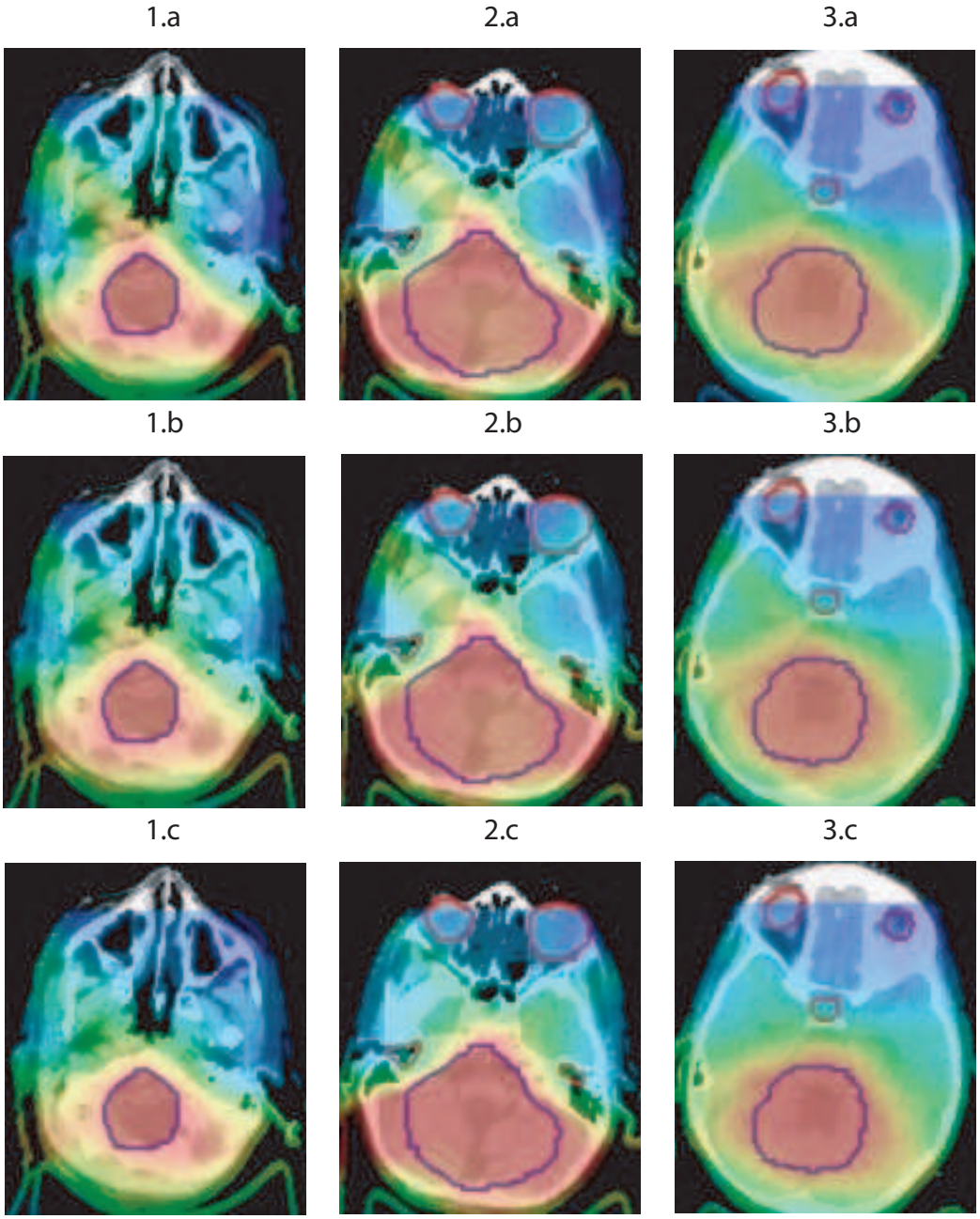

Figure 1: Brain Case Dose Distribution: (a) Basic 8 Equi-spaced Beams Solution, (b) Final 8 Equi-Spaced Beams Solution, (c) Final 8 Selected Beams Solutions are shown with a colorwash dose distribution overlaid with three CT axial images. The prescription dose is shown as red colorwash with 75, 50 and 25% of prescription dose shown as yellow, green and blue colorwash. CT axial images 1, 2, and 3 represent inferior, mid and superior slices through the target volume shown as a blue contour. The red contours represent the eyes. The cochlea structures are shown on slice 2 in red, and the pituitary is shown as red contour on slice 3.

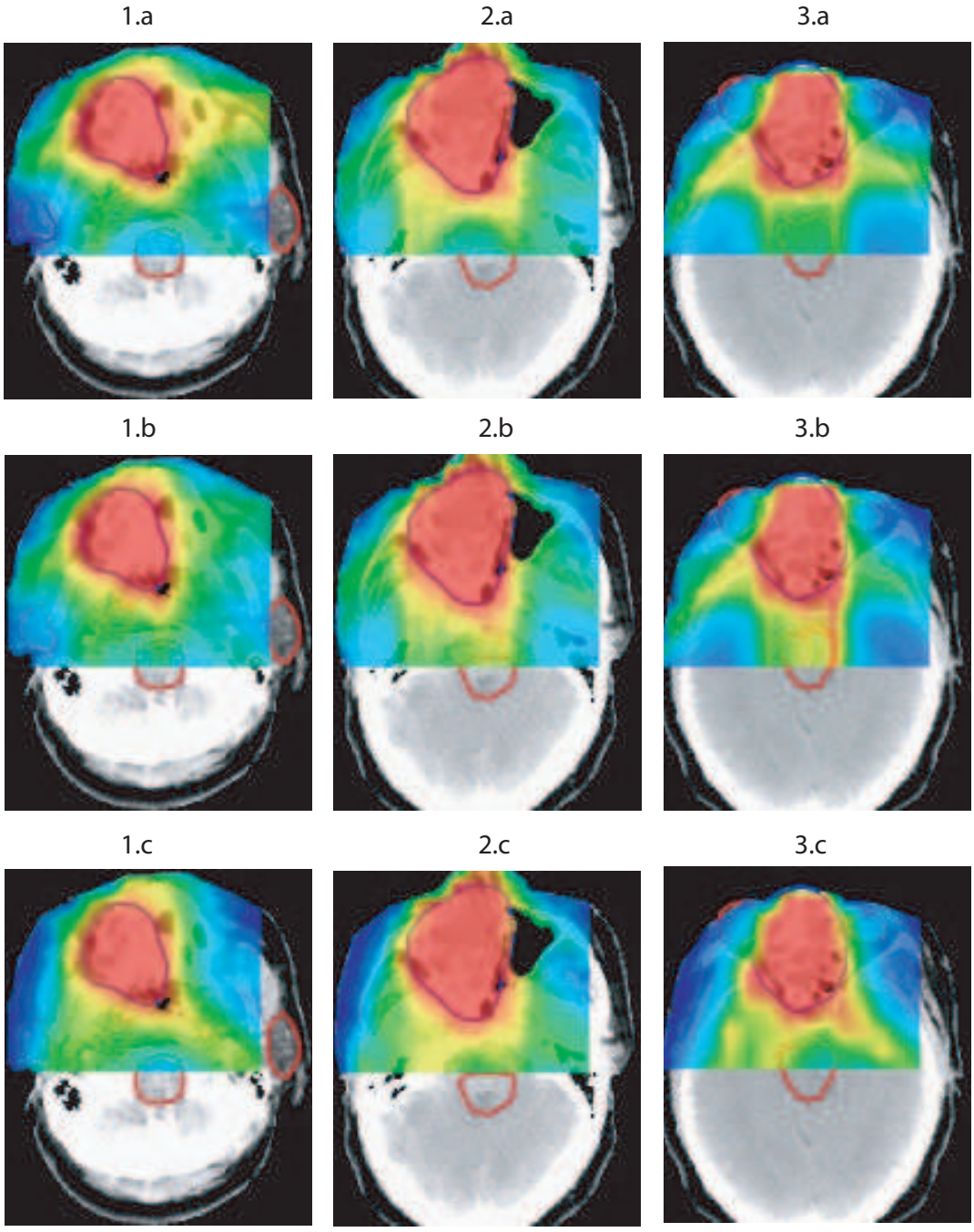

Figure 2: Head and Neck Case Dose Distribution: (a) Basic 8 Equi-spaced Beams Solution, (b) Final 8 Equi-Spaced Beams Solution, (c) Final 8 Selected Beams Solution are shown with a colorwash dose distribution overlaid with three CT axial images. The prescription dose is shown as red colorwash with 75, 50 and 25% of prescription dose shown as yellow, green and blue colorwash, respectively. CT axial images 1, 2, and 3 represent inferior, mid and superior slices through the target volume shown as a blue contour. The red central contour represents the brainstem as a critical structure. Slice 3 shows the critical structure *Globe_RT* right next to the target structure which contributes to a cold spot issue.

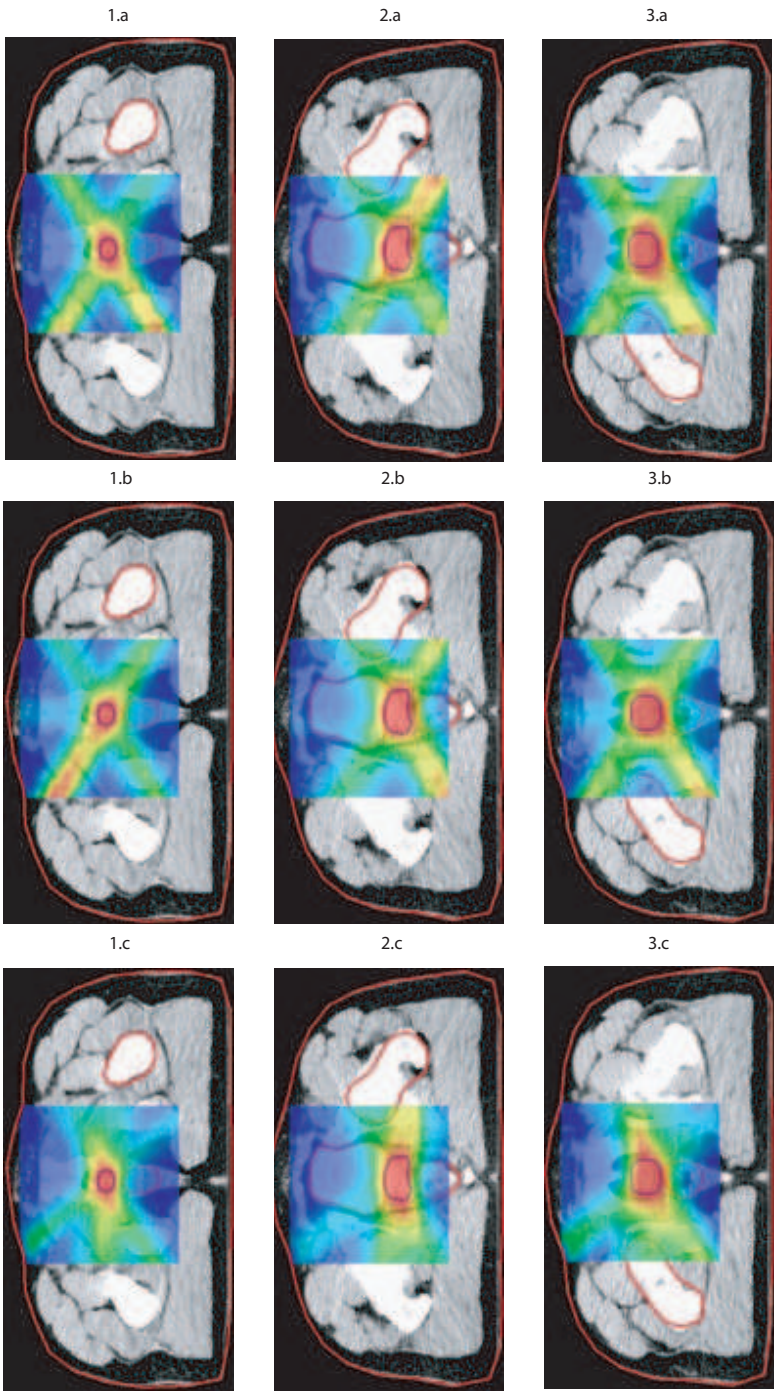

Figure 3: Prostate Case Dose Distribution: (a) Basic 6 Equi-spaced Beams Solution, (b) Final 6 Equi-Spaced Beams Solution, (c) Final 6 Selected Beams Solution are shown with a colorwash dose distribution overlaid with three CT axial images. The prescription dose is shown as red colorwash with 75, 50 and 25% of prescription dose shown as yellow, green and blue colorwash, respectively. CT axial images 1, 2, and 3 represent inferior, mid and superior slices through the prostate shown as a blue contour. The red contours on slice 2 show the bladder and rectum structures.

	4 beams		5 beams		6 beams	
	pBEV	Proposed Scheme	pBEV	Proposed Scheme	pBEV	Proposed Scheme
Coverage	1.000	1.000	1.000	1.000	1.000	1.000
Conformity	1.050	1.029	1.046	1.038	1.038	1.033
Coldspot	1.000	1.000	1.000	1.000	1.000	1.000
Hotspot	1.150	1.150	1.150	1.150	1.150	1.150

Table 3: Prostate case comparison to pBEV